

# The Interannual Variability of Summer Rainfall in the Arid and Semiarid Regions of Northern China and Its Association with the Northern Hemisphere Circumglobal Teleconnection

HUANG Gang<sup>\*1,2</sup> (黄刚), LIU Yong<sup>2,3</sup> (刘永), and HUANG Ronghui<sup>2</sup> (黄荣辉)

<sup>1</sup>Key Laboratory of Regional Climate-Environment Research for Temperate East Asia,  
Institute of Atmospheric Physics, Chinese Academy of Sciences, Beijing 100029

<sup>2</sup>State Key Laboratory of Numerical Modeling for Atmospheric Sciences and  
Geophysical Fluid Dynamics, Center for Monsoon System Research,  
Institute of Atmospheric Physics, Chinese Academy of Sciences, Beijing 100083

<sup>3</sup>Graduate University of Chinese Academy of Sciences, Beijing 100049

(Received 17 December 2009; revised 8 May 2010)

## ABSTRACT

Using the latest daily observational rainfall datasets for the period 1961–2008, the present study investigates the interannual variability of June–September (JJAS) mean rainfall in northern China. The regional characteristics of JJAS mean rainfall are revealed by a rotated empirical orthogonal function (REOF) analysis. The analysis identifies three regions of large interannual variability of JJAS rainfall: North China (NC), Northeast China (NEC), and the Taklimakan Desert in Northwest China (TDNWC). Summer rainfall over NC is shown to have displayed a remarkable dry period from the late 1990s; while over NEC, decadal-scale variation with a significant decreasing trend in the last two decades is found, and over TDNWC, evidence of large interannual variability is revealed. Results also show that the interannual variability of JJAS rainfall in northern China is closely associated with the Northern Hemisphere circumglobal teleconnection (CGT). Correlation coefficients between the CGT index and regional-averaged JJAS mean rainfall over NC and NEC were calculated, revealing values of up to 0.50 and 0.53, respectively, both of which exceeded the 99% confidence level.

**Key words:** rotated empirical orthogonal function analysis, arid, semiarid, interannual variability, circumglobal teleconnection

**Citation:** Huang, G., Y. Liu, and R. H. Huang, 2011: The interannual variability of summer rainfall in the arid and semiarid regions of northern China and its association with the northern hemisphere circumglobal teleconnection. *Adv. Atmos. Sci.*, **28**(2), 257–268, doi: 10.1007/s00376-010-9225-x.

## 1. Introduction

The arid and semi-arid regions (ASAR) of China, mainly located in the north, cover nearly half of the land area (e.g. Chen et al., 2009). The annual rainfall in these regions is almost less than 400 mm. The amount of rainfall in most parts of ASAR, during the rainy months of June, July, August, September (JJAS), accounts for more than 70% of annual rainfall (Fig. 1). Rainfall is an essential component of the

water balance. Its anomalies have crucial effects on industry and agriculture, as well as the lives of people, particularly for ASAR in China. Previous studies have shown signs of severe desertification and persistent drought in the semiarid region of northern China in recent decades (Wang and Li, 1990; Yatagai and Yasunari, 1994; Huang et al., 1999; Huang, 2006). The local and remote effects of the land surface processes and land degradation over ASAR in northern China have also been discussed in observational and numer-

---

\*Corresponding author: HUANG Gang, hg@mail.iap.ac.cn

ical studies (e.g. Xue, 1996; Zhang et al., 2005; Zhou and Huang, 2006). These studies have indicated that variations in land-surface sensible flux and land degradation can cause local and remote rainfall anomalies. In turn, rainfall anomalies will affect land surface processes and cause changes to the environment. Therefore, identifying the long-term and interannual variability of rainfall and understanding the underlying mechanisms are of great importance to the future development of the economy, not only in ASAR, but also for other parts of the East Asian monsoon region. Much effort has been applied in studying summer rainfall variability in northern China during recent decades. Such work can generally be divided into two aspects, based on the domain of interest: persistent drought in North China, and the climate variations of ASAR in Northwest China.

For the first aspect, many previous studies have in-

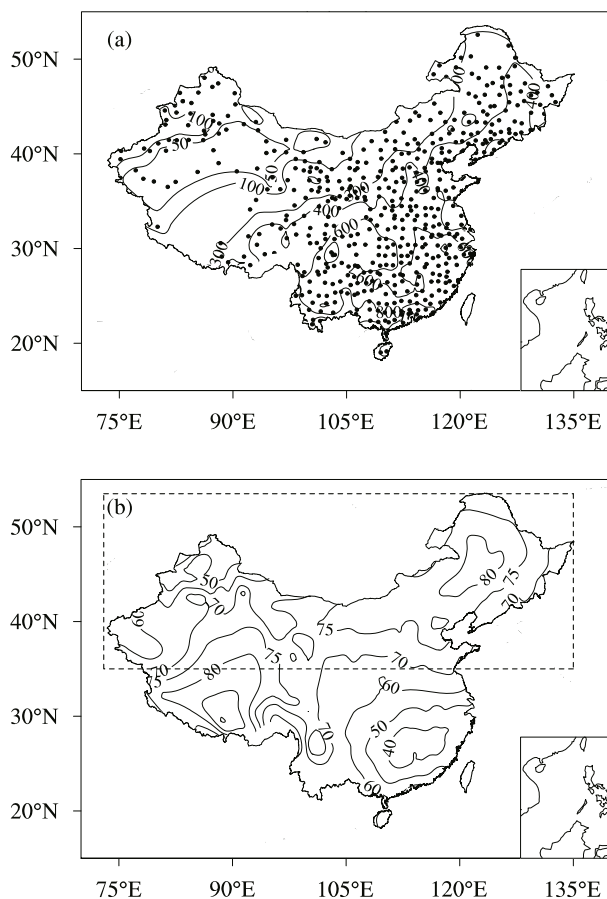


**Fig. 1.** (a) Geographical distribution of mean JJAS total precipitation (mm) and (b) the ratio (%) of JJAS mean rainfall to annual mean rainfall in China for the period 1961–2008. Dots in (a) denote the 552 weather stations. The dashed rectangular area represents the domain covered in the study.

dicated there exists a decadal shift and a significant decreasing trend in summer precipitation over North China since the mid-1970s (Wang and Li, 1990; Chen et al., 1992; Yatagai and Yasunari, 1994; Yatagai and Yasunari, 1995; Nitta and Hu, 1996; Huang et al., 1999; Li et al., 2002; Gong et al., 2004; Xu et al., 2005; Ding et al., 2008; Huang et al., 2008). Wang and Li (1990) documented a possible link between precipitation fluctuations over the semiarid region of northern China and the summer monsoon, the western Pacific subtropical high, and ENSO. Huang et al. (2008) put forward a schematic model for how the interdecadal variations of the East Asian Climate system cause the persistent drought in North China, which is associated with ENSO, the subtropical High, mid-latitude wave train activity, Tibetan Plateau snow, and land surface processes. They proposed that the East Asian monsoon system was a coupling system of atmosphere, ocean, and land, and that the drought in North China (NC) was affected by the variability of East Asian monsoon climate subsystems, as well as their interaction between each other.

For the second aspect, many observational studies have revealed that summer rainfall in Northwest China (NWC) shows an increasing trend since the 1960s, with a remarkable shift in the mid-1970s (Yatagai and Yasunari, 1994, 1995; Gong et al., 2004; Endo et al., 2005; Ma and Fu, 2006; Shi et al., 2007; Yang and Zhang, 2008; Zhou and Huang, 2009). These studies have also indicated that summer rainfall change in NWC exhibits regional characteristics, with a stage of relative increase in western parts of NWC, but a stage of drought in eastern parts, and that the intensity of the increasing trend of summer rainfall is greater in northern Xinjiang than in southern Xinjiang. Yang and Zhang (2008) analyzed the relationships between summer rainfall in Xinjiang and the Asian subtropical westerly jet stream (ASWJS). They revealed that the summer rainfall anomaly in Xinjiang had a notable correlation to the position of the ASWJS, as well as quasi-stationary wave activity. Zhou and Huang (2009) investigated the possible cause of interdecadal variability in summer rainfall in NWC and pointed out that an increase in near-surface temperature after 1978 enhanced convective instability, which in turn contributed to a strengthening of ascent and an increase in summer rainfall in NWC during the period 1978–2000.

ASAR has a large span in the east–west direction. The rainfall anomaly pattern in this region may mirror large-scale characteristics of atmospheric circulation and indicate internal connections between different parts. However, most previous work has focused on decadal-scale rainfall variability and on one part

of ASAR only. Few studies have addressed climatic variations over ASAR as a whole, which may provide essential information for understanding the nature of desertification in northern China. Therefore, one of the aims of the present paper is to investigate the interannual variability and regional characteristics of JJAS mean precipitation, and the associated atmospheric circulation, across the whole of ASAR.

The influence of atmospheric teleconnection on boreal summer climate has been studied extensively. For example, a study by Nitta and Hu (1996) indicated that the Pacific–Japan (PJ) and Eurasia teleconnection patterns (EU) play very important roles in the variation of coupled patterns of summer rainfall and temperature in China, especially along the middle-lower reaches of the Yangtze River. More recent studies have suggested that the EU teleconnection is a bridge connecting the Indian summer monsoon (ISM) and the East Asian summer monsoon (EASM) (e.g. Wang et al., 2001; Wu and Wang, 2002). Lu et al. (2002) indentified a teleconnection pattern in July emerging from North Africa to East Asia along the westerly jet in the middle latitudes. They suggested that the teleconnection is a possible linkage of the EASM to the Indian monsoon, and even to subtropical heating anomalies over the Atlantic. Ding and Wang (2005) revealed a recurrent CGT pattern in the summertime mid-latitude circulation in the Northern Hemisphere. The CGT, actually a combination of the ISM–EASM teleconnection, the Silk-Road, and the Tokyo–Chicago express, is accompanied by significant rainfall and surface temperatures in the continental regions of Western Europe, European Russia, India, East Asia, and North America. ASAR is mainly located between  $35^{\circ}\text{N}$  and  $55^{\circ}\text{N}$ , which is on the path of the CGT. As revealed in this paper, the dominant mode of the JJAS mean rainfall in ASAR is closely associated with the CGT, which may suggest a new way to understand drought in northern China.

The remainder of the text is organized as follows. The datasets and methodology used are described in section 2. Section 3 presents the spatial and temporal variations of JJAS mean rainfall in northern China. In section 4, the relationship between the upper-level circumglobal teleconnection and JJAS rainfall in China is examined. A discussion is provided in section 5. And finally, conclusions are summarized in section 6.

## 2. Data and methods

### 2.1 Datasets

Two major datasets were used in this study. The first comprised daily observational rainfall data from 828 weather stations, and was provided by the Na-

tional Meteorological Information Center of China, spanning the period 1951–2008. To achieve temporal continuity in terms of coverage from each station, we chose 552 stations (dots in Fig. 1a) from the complete data archive, as well as a slightly shorter period spanning 1961–2008 for this study. The second dataset comprised monthly atmospheric data for the period 1961–2008 from the National Centers for Environmental Prediction–National Center for Atmospheric Research (NCEP–NCAR) reanalysis (Kalnay et al., 1996), on a horizontal resolution of  $2.5^{\circ}\times 2.5^{\circ}$ . The variables used in this study included winds and height at the 200, 500, 700, and 850 hPa levels.

### 2.2 Methods

As already mentioned, the present study concerns the area of northern China; however, more specifically, this covers the domain ( $35^{\circ}$ – $55^{\circ}\text{N}$ ,  $73^{\circ}$ – $136^{\circ}\text{E}$ ), which includes a total of 273 weather stations (area denoted by the dashed rectangle in Fig. 1b). The rotated empirical orthogonal function (REOF) method of analysis was applied to reveal the regional characteristics of interannual variations in JJAS mean precipitation over the domain concerned. Firstly, the station datasets were normalized and long-term trends removed. Then, a correlation matrix of the rainfall data was used to compute the eigenvalues and eigenvectors of EOFs. After that, the first three EOFs were rotated orthogonally from the six leading modes of EOFs. Regression and correlation analysis were also used, in order to study the relationship between the interannual variation of JJAS rainfall in northern China and general atmospheric circulations.

## 3. Spatial and temporal variations of JJAS mean rainfall in northern China

### 3.1 Long-term trend of JJAS mean rainfall in northern China (1961–2008)

This study employed a relative variation ratio (RVR) to indicate the extent of change in JJAS mean rainfall during the period 1961–2008 in northern China. The RVR was obtained by dividing the linear trend of JJAS mean rainfall of one station by the JJAS mean rainfall of that station. The distribution of RVR in China is displayed in Fig. 2. A notable west–east contrast, with rainfall increasing in most parts of NWC, but decreasing in NC, Northeast China (NEC), can be observed. Furthermore, the largest positive and negative centers exist in North Xinjiang, and NC, respectively. These results are consistent with previous studies.

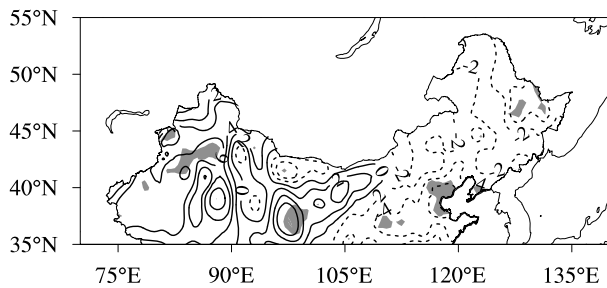


**Fig. 2.** RVR (%) of JJAS mean rainfall in northern China over the period 1961–2008 [units:  $\text{mm} (10 \text{ yr})^{-1}$ ]. Shading indicates regions with trend anomalies beyond the 90% confidence level.

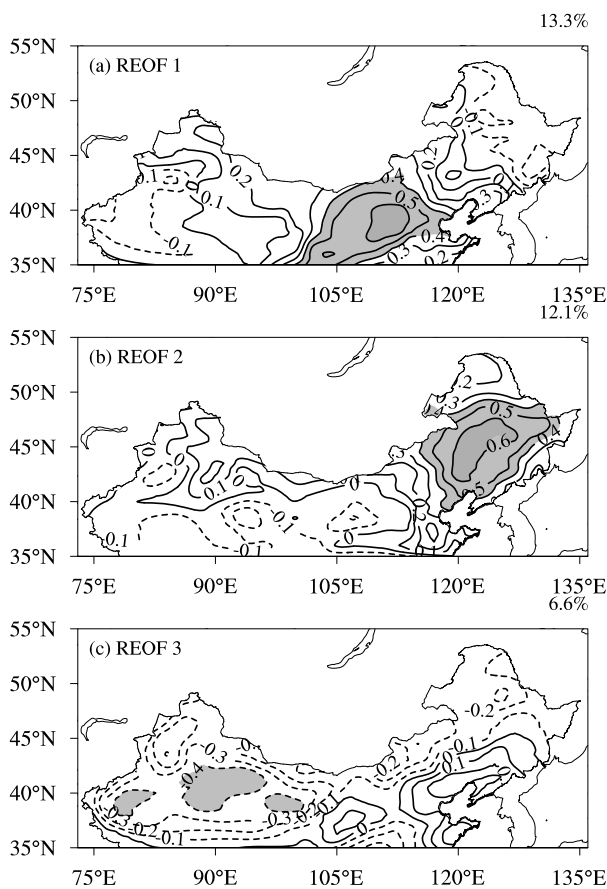


**Fig. 3.** Spatial modes of the first three REOFs of JJAS mean rainfall anomalies in northern China (contour interval: 0.1). Shaded areas indicate regions with values beyond 0.4 and less than  $-0.4$ . The contribution of each mode to the total variance is displayed in the upper right of each panel.

### 3.2 Spatial and temporal variation of JJAS mean rainfall in northern China (1961–2008)

To investigate the interannual variation in JJAS mean precipitation in northern China, REOF analysis,

a widely used diagnostic tool in climatology, was applied. It retains the advantages but avoids the spatial limitations of EOF analysis, and can reveal efficiently the regionality of climatic factors (e.g. Richman, 1986; Murata, 1990; Yatagai and Yasunari, 1995; Li et al., 2002). The spatial patterns of the first three leading REOFs of the JJAS mean rainfall in northern China are shown in Fig. 3. The three modes account for 13.3%, 12.1%, and 6.6% of the total variance, respectively. The first two REOF modes feature a quasi-zonal tripole-like distribution with an anomalous center over the horseshoe-shaped arc region and adjacent region in between. The pattern in Xinjiang Province shows an opposing north–south distribution, which agrees with Yang and Zhang (2008). The third mode displays a consistent anomalous pattern in most

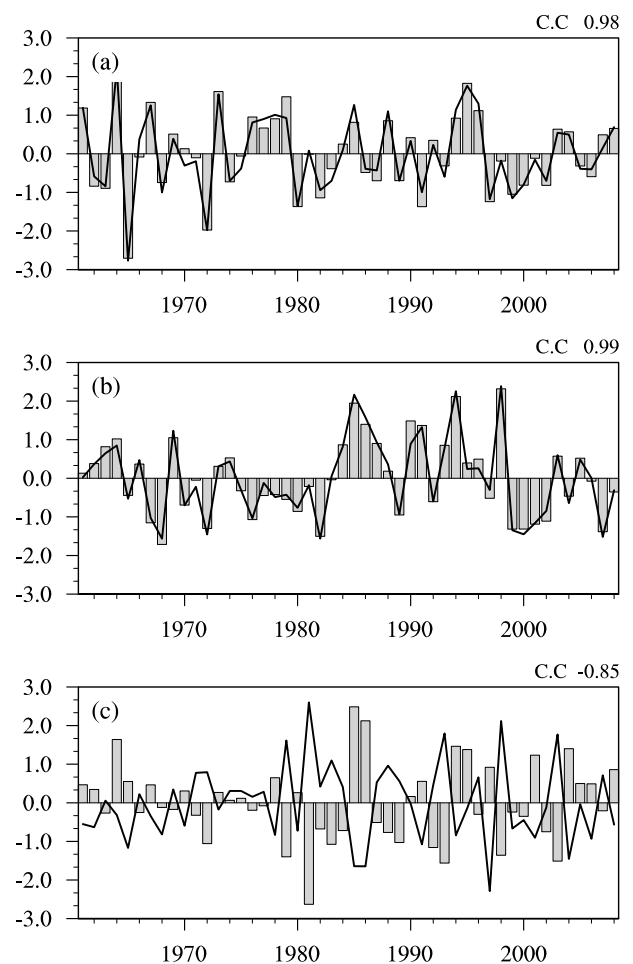


**Fig. 4.** Normalized time coefficients of each REOF mode [histograms: (a) for REOF1, (b) REOF2, and (c) REOF3] and the normalized series of regional mean JJAS rainfall for each relevant region [solid lines: (a) for NC, (b) NEC, and (c) TDNWC]. And the correlation coefficient (C.C) between the two time series in each subpanel is also added in its upper right.

parts of northern China, especially in NWC.

The spatial distribution in Fig. 3 designates the correlation coefficients of JJAS mean rainfall anomalies at each station with the time series corresponding to the REOF modes. The shaded areas, with values beyond 0.4 or less than  $-0.4$ , denote the correlation coefficients exceeding the 99% confidence level. So, three regions (shaded in Fig. 3) associated with the three dominant modes can be deduced: most parts of NC, NEC, and the Taklimakan Desert region in northwest China (TDNWC), with 76, 67, and 28 weather stations in each region, respectively.

The corresponding time coefficient of each principle component (PC) to the three REOF modes (histogram) and the JJAS mean rainfall anomalies over the regions of NC, NEC, and TDNWC (solid lines) are depicted in Fig. 4. It is obvious that the three PCs match well with the regional averaged JJAS mean rainfall anomaly of the associated region. The correlation coefficients between the three pairs of time series are 0.99, 0.98, and  $-0.86$ , respectively, all beyond the 99% confidence level based on Pearson's  $r$  statistical significance test. Thus, the three PCs characterize JJAS mean rainfall variability of the corresponding region. Furthermore, by combing the power spectrum of each PC (Fig. 5), each of their features of variability can be obtained. PC1 exhibits a 3- and 9-year periodic variation, showing a remarkable relatively dry period from the mid-1990s to the present day. PC2 shows decadal-scale variation and a distinct decreasing trend in the last two decades, with dry periods from the late 1960s to the early 1980s, and from the late 1990s to the present day, and with wet periods between. Meanwhile, there is no significant frequency

based on the spectral analysis, as shown by Fig. 5b. For the third PC, the spectral analysis result reveals large interannual variability, with 4-5- and 9-year periods of variation (Fig. 5c).

#### 4. The relationship between the CGT and interannual variations of JJAS mean rainfall in northern China

The CGT is a geographically phase-locked recurrent teleconnection pattern during boreal summer from July to September, having its path within the westerly jet stream from the Northeast Atlantic through Eurasia, the North Pacific, to North America, and having three center cells primarily in East Asia, mainly in northern China (Ding and Wang, 2005). Interestingly, the interannual variability of JJAS mean rainfall in northern China shows a clear quasi-zonal wave-like distribution in the first two REOFs, with the center over a horseshoe-shaped arc region, where the transition area of ASAR is located. It is conceivable that the first two leading REOFs may have a potential connection with the CGT. This section investigates this relationship.

##### 4.1 The CGT patterns associated with the first two leading modes of JJAS mean rainfall in northern China

To begin with, the atmospheric circulation anomalies corresponding to the first two dominant modes of the REOFs are explored using the regression method. Figure 6 shows the regressed patterns of JJAS mean height at the 200 hPa and 700 hPa levels with respect to the first two time coefficients mentioned above. The

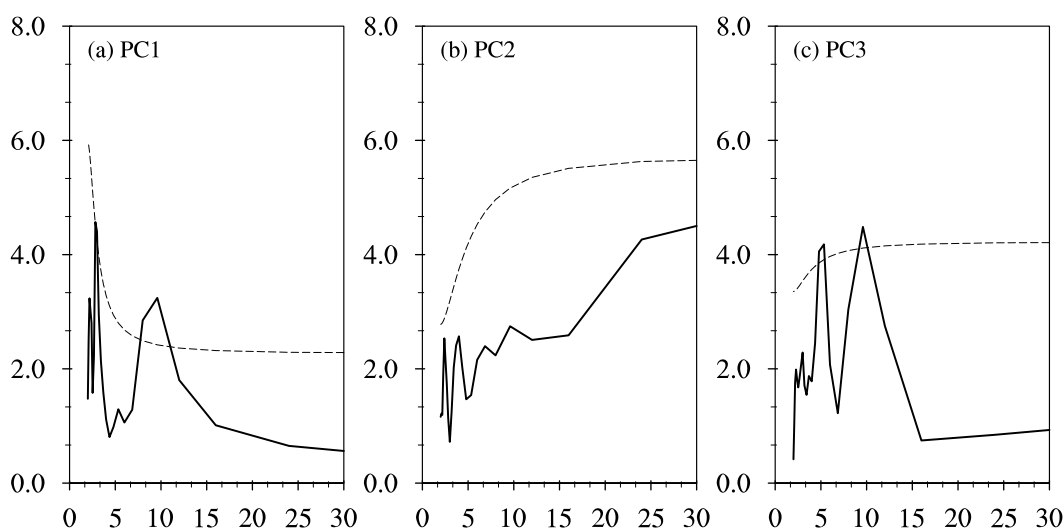


**Fig. 5.** The power spectrum (solid line) for the principle component (PC) of the three REOFs, and the dotted thin lines represent the power spectrum at the 95% confidence level.

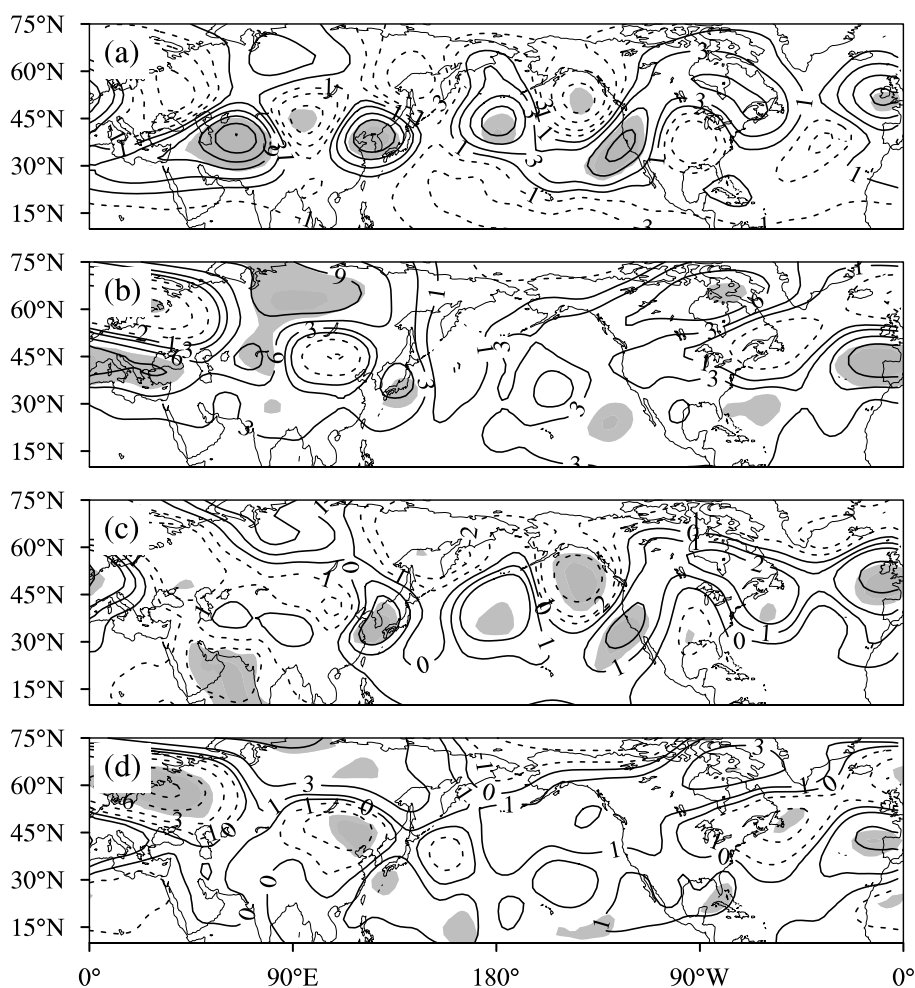


**Fig. 6.** Anomalies of regressed geopotential height at 200 hPa (a, b) and 700 hPa (c, d). (a, c) against PC1; (b, d) against PC2. Shading represents regions with height anomalies beyond the 95% confidence level.

most prominent feature in Fig. 6a, which is related to PC1 regressed onto the height at 200 hPa, is a wave train structure from the Northeast Atlantic through Eurasia, the North Pacific, to North America, with positive anomalous centers over the Northeast Atlantic, central Asia, Northeast Asia, the central-north Pacific, and western North America, with negative centers between. The largest positive center is found over central Asia in the domain ( $35^{\circ}$ – $40^{\circ}$ N,  $60^{\circ}$ – $70^{\circ}$ E).

The regressed height pattern at the 200 hPa level against PC2 is shown in Fig. 6b. A similar wave train structure emerges, although not as clear and strong as that in Fig. 6a, especially over the North Pacific and North America. The positions of the anomalous centers move a little eastward compared to those in Fig. 6a. In addition, a NAO-like (North Atlantic Oscillation) pattern presents along the coastline of Western Europe from North Africa to the North Atlantic, sug-

gesting influence from the high latitudes.

The atmospheric circulation at the 500 hPa level related to the two REOF modes exhibits a good similarity to that at the 200 hPa level (Figs. 6a, b), having anomalous centers over the same locations, but the amplitude of the anomalies increases with height (figures not shown).

The regressed geopotential height anomalies at 700 hPa corresponding to the two REOFs modes are shown in Figs. 6c and d. The regressed low-level height anomalies exhibit wave train patterns similar to those shown in Figs. 6a and b, though with weaker intensity and a tilted baroclinic structure over the northwest part of India where there is an anomalous ridge at 200 hPa and an enhanced cyclonic anomaly over the Arabian Peninsula and adjacent sea at 700 hPa. The regressed wind fields against the two REOF modes match the height anomalies well (figure not shown).

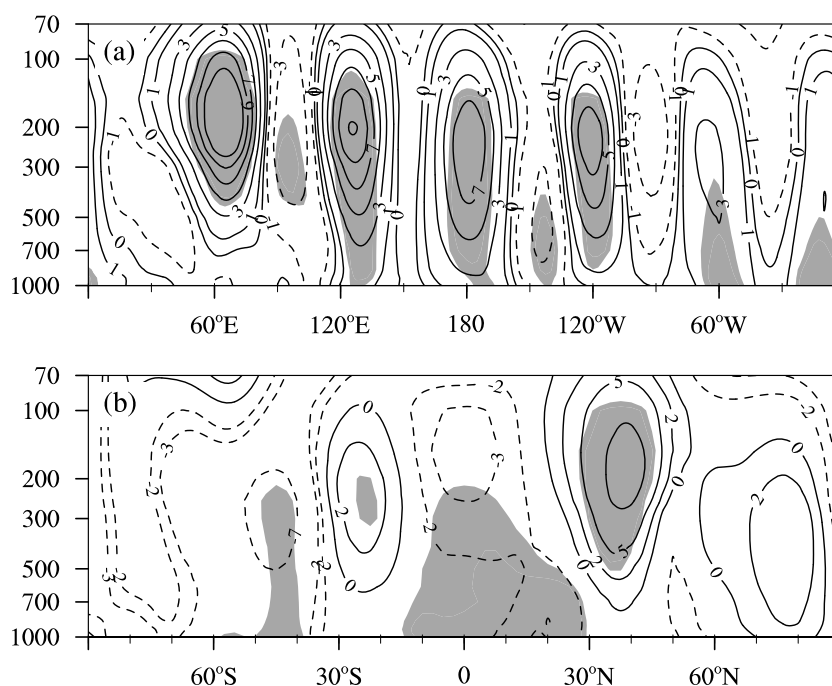


**Fig. 7.** (a) Height–longitude cross-section anomalies of PC1 regressed onto height averaged within  $30^{\circ}$ – $50^{\circ}$ N. (b) Height–latitude cross-section anomalies of PC1 regressed onto height averaged within  $60^{\circ}$ – $70^{\circ}$ E. Shaded reveals the regions with height anomalies exceed the 90% confidence level.

The vertical structure of the wave train pattern can also be examined. Figure 7a illustrates the height–longitude cross section anomalies of PC1 regressed onto height averaged within  $30^{\circ}$ – $50^{\circ}$ N. Evidently, a wave train structure emerges along the westerly jet from near  $60^{\circ}$ E, passing over Eurasia to North America. This wave-like pattern shows a vertically quasi-barotropic structure for nearly all the wave train centers, except for a tilted baroclinic pattern over the northwest part of India. Also, it has a wavenumber-6 structure, with an intense region of positive/negative anomalous centers confined to  $30^{\circ}$ – $50^{\circ}$ N within a waveguide associated with the westerly jet stream extending from Eurasia to North America. Furthermore, it is evident that the maximum anomalous center for each cell is at about the 200 hPa level, with the largest one occurring around  $65^{\circ}$ E. These features demonstrate a geographically fixed global-scale teleconnection pattern, strikingly similar to the CGT revealed in Ding and Wang (2005). Moreover, the regressed patterns at 200 hPa are identical to the two scenarios of the CGT proposed by Ding and Wang (2005) [see Fig. 15 in Ding and Wang (2005)], respectively. These similarities can be clearly seen in Fig. 8.

Figure 8 displays the meridional wind anomalies associated with the first two PCs. The pattern corresponding to PC1, as shown in Fig. 8a, exhibits

an apparent wave-like structure propagating within the westerly jet stream from the Northeast Atlantic, through Eurasia and the North Pacific, to eastern America, and for the regressed pattern against PC2 shown in Fig. 8b, a notable teleconnection pattern emerges over the Eurasian continent from Northern Europe to East Asia. Additionally, a distinct discrepancy is observed over the Arctic region in which the magnitude of anomalies regressed against PC1 are much weaker than those against PC2. This implies that the strong anomalous activity over the Arctic area, or from high latitudes, may affect the wave-like anomaly pattern. The features revealed in Fig. 8 matches well with Ding and Wang (2005).

#### 4.2 JJAS rainfall anomalies in China associated with CGT patterns

The results thus far have indicated that the interannual variability of JJAS mean rainfall in northern China shows a considerable correlation with the CGT pattern. Here, following Ding and Wang (2005), the correlation distributions between them are examined. First, two indices, CGTI-1 and CGTI-2, are defined to represent the two scenarios of CGT variability, respectively.

For the first scenario, we employ the definition by Ding and Wang (2005), which is defined as the norma-

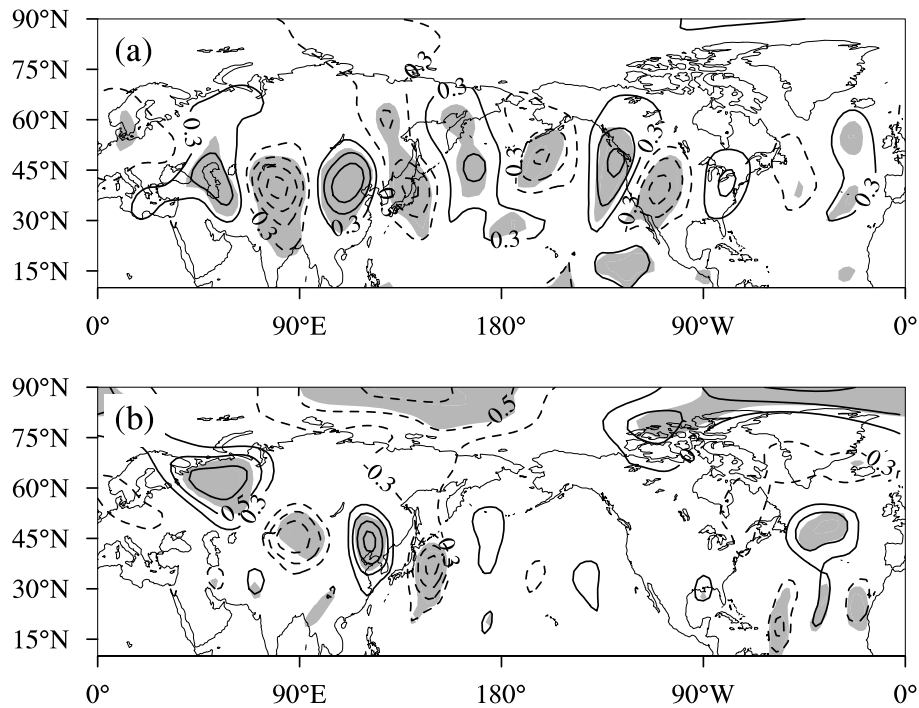


**Fig. 8.** Anomalies of JJAS mean meridional wind at 200 hPa regressed against PC1 (a) and PC2 (b). Shallow area indicates the region with wind anomalies beyond the 95% confidence level.

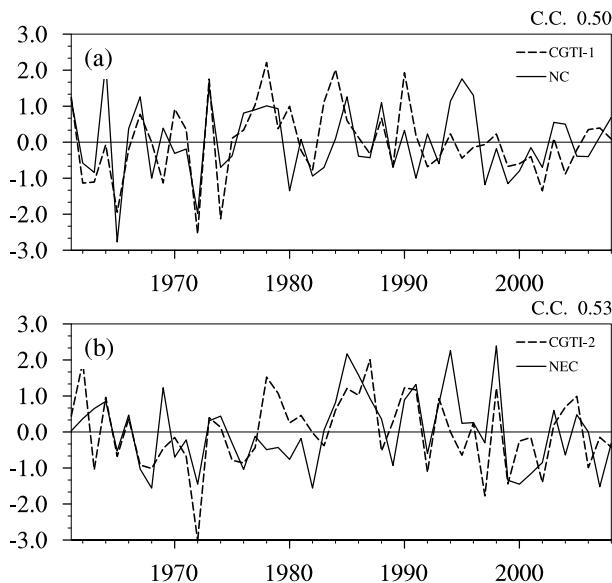


**Fig. 9.** Normalized time series of CGTI 1-2 (dashed lines) and regional mean JJAS rainfall in NC and NEC (solid lines). And the correlation coefficient (C.C) between each pair of time series is also added in the upper right of each panel.

alized time series of the interannual variability of the 200 hPa height averaged over the reference area ( $35^{\circ}$ –

$40^{\circ}$ N,  $60^{\circ}$ – $70^{\circ}$ E), and denote it as CGTI-1. CGTI-2, corresponding to the second scenario, is defined using the difference between the normalized time series of regionally-averaged height at 200 hPa over the two areas, ( $40^{\circ}$ – $50^{\circ}$ N,  $20^{\circ}$ – $10^{\circ}$ W) and ( $60^{\circ}$ – $65^{\circ}$ N,  $15^{\circ}$ – $25^{\circ}$ E). The regressed height anomalies at 200 hPa against the two indices resemble those in Fig. 6 (figures not shown).

Figure 9 displays the two indices and the normalized time series of regionally-averaged JJAS mean rainfall in NC and NEC. The correlation coefficients between the two pairs of time series are 0.50 and 0.53, respectively, both beyond the 99% confidence level. The correlation coefficients of the JJAS mean rainfall and the two CGTIs are displayed in Fig. 10, the patterns of which resemble the spatial modes of the first two REOFs (Figs. 3a, b), with significant anomalies located in northern China, especially NC, NEC, and western part of Xinjiang Province. The composite atmospheric circulations related to the CGTIs are also performed. Figure 11 shows the positive-minus-negative CGTI composite wind anomalies at 850 hPa (vector) and vertical velocities at 500 hPa (contour), the cases of which are chosen from the lower and upper bounds, respectively, with a 0.5 standard deviation of the CGTIs. The composite results show that, corresponding to each scenario, an anomalous southerly

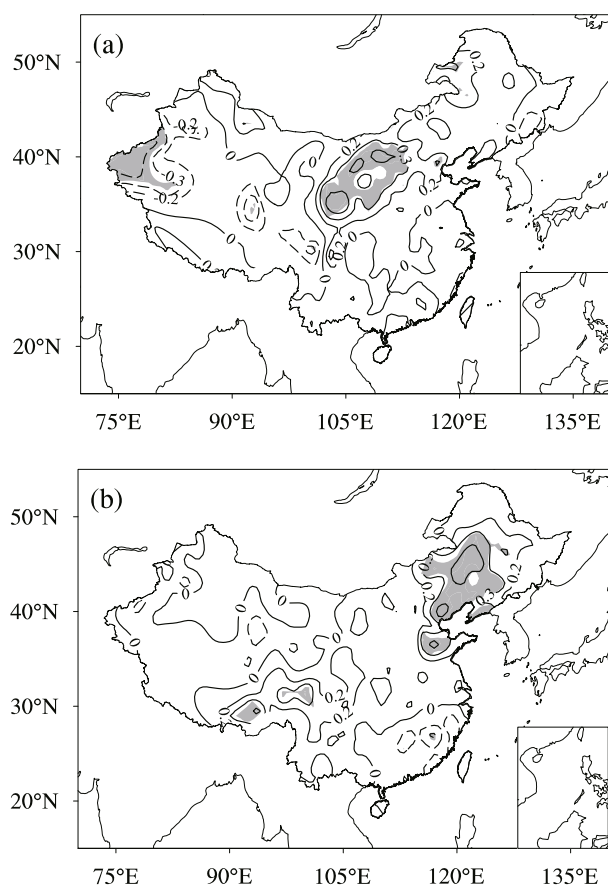


**Fig. 10.** Correlation coefficients between CGTI and the JJAS mean rainfall in China: (a) CGTI-1; (b) CGTI-2. Shaded area illustrates the region of rainfall anomalies beyond the 95% confidence level.

over Eastern China with abundant moisture flows to northern China converges with the cold air from high latitudes and triggers anomalous ascending motion over NC/NEC, all of which are most favorable for the occurrence of rainfall, and thus positive rainfall anomalies are found over the two regions. Meanwhile, both the two CGTIs and the rainfall anomalies in NC/NEC are in a below-normal phase during recent decades. As to why this happens requires further study.

## 5. Discussion

Previous studies have already revealed that there are teleconnection patterns and stationary Rossby waves propagating eastward within the Asian jet in boreal summer (e.g. Ambrizzi et al., 1995; Rodwell and Hoskins, 1996; Krishnan and Sugi, 2001; Lu et al., 2002; Wu and Wang, 2002; Enomoto et al., 2003; Enomoto, 2004; Ding and Wang, 2005; Sato and Takahashi, 2006) and these features can be achieved by a

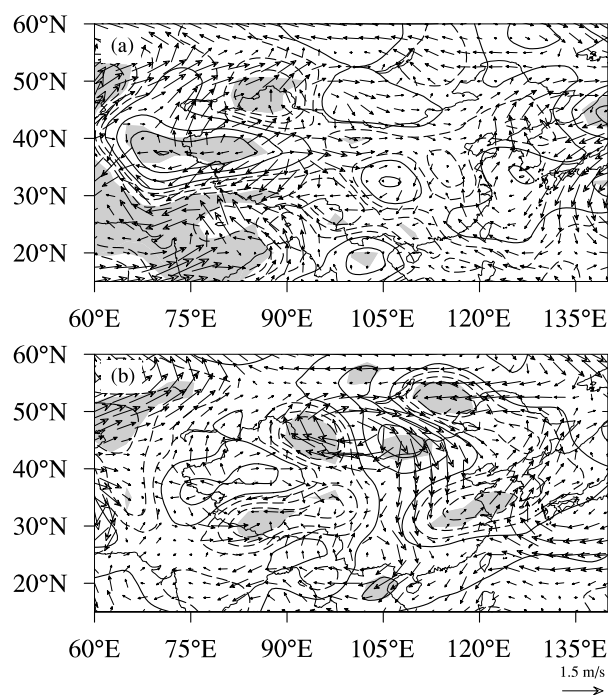


**Fig. 11.** Composite anomalies of winds (vectors, arrow with scale at bottom right of the panels) at 850 hPa and vertical velocity (contour) at 500 hPa associated with the two CGTIs: (a) CGTI-1; (b) CGTI-2. Shading denotes the region with vertical velocity anomalies beyond the 95% confidence level.

few variables, such as geopotential height, streamfunction, and meridional wind. The formation mechanism of the wave-like pattern on the jet has also been discussed (Rodwell and Hoskins, 1996; Enomoto et al., 2003; Ding and Wang, 2005; Sato and Takahashi, 2006; Shi and Lu, 2010). Rodwell and Hoskins (1996) revealed that the diabatic heating associated with the Indian monsoon resulted in diabatic cooling and downward motion over the Eurasian continent and Mediterranean Sea. A study by Enomoto et al. (2003) indicated that heating from the Indian monsoon and the related diabatic forcing over the continent would excite a quasi-stationary disturbance on the jet, triggering a barotropic structure propagating within the westerly jet. Sato and Takahashi (2006) reported that a Rossby wave packet propagated eastward from the Middle East, passing over East Asia, and reaching North America. They showed that the anomaly pattern was strengthened through kinetic energy conversion near the entrance of the Asian jet over the Middle East, and that the interaction between the anomaly pattern and the basic field contributed to the appearance of the anomalous wave-like pattern.

Most of the studies mentioned above discuss the teleconnection pattern on the monthly or submonthly

timescale. On the seasonal scale, the features of the teleconnection also, to some extent, reveal the possible relationship between the teleconnection and associated factors mentioned above, such as the westerly jet (shown in Fig. 7a) and the heating from the ISM. Figure 7a shows a clear wave train pattern propagating eastward along the westerly jet, which plays the role of the waveguide confining the wave train to within the domain  $30^{\circ}$ – $50^{\circ}$ N. Furthermore, interestingly, the teleconnection pattern exhibits an evident baroclinic structure around  $65^{\circ}$ E, with a maximum center at about 200 hPa. Thus the vertical structure around  $65^{\circ}$ E is investigated. Figure 7b depicts the height–latitude cross section of geopotential height anomalies (averaged within the domain  $50^{\circ}$ – $70^{\circ}$ E) regressed against PC1. A barotropic teleconnection pattern appears with out-of-phase anomalies between the tropics and extratropics, especially in the Northern Hemisphere. This structure can also be seen in Fig. 11a, where the vertical velocity anomalies at 500 hPa show an “ascent–descent–ascent” pattern around  $65^{\circ}$ E. Furthermore, we can determine that the meridional teleconnection pattern may be closely related to the low level activity over the Indian Continent/Ocean, where significant height anomalies are apparent. This meridional teleconnection pattern resembles the low-frequency waveguide (or a biweekly oscillation) at 200 hPa near  $60^{\circ}$ E, mentioned in Liu and Yu (1993). These authors documented that the wave source of this waveguide was located around  $10^{\circ}$ – $25^{\circ}$ N, and the perturbation propagated polarward from the wave source to affect the westerlies of the Southern and Northern Hemispheres. This indicates that the waveguide near  $60^{\circ}$ E may be a bridge connecting the tropics and extratropics. Wang et al. (2005) proposed a mechanism for how the tropical activity affected the extratropical atmosphere. They indicated that a forcing embedded in the deep tropical easterlies may excite a Rossby wave response in the extratropical westerlies and the southerly flow component in the basic state played a role of a conveyor, transferring a Rossby wave source northward. The study by Wang et al. (2005) also showed that the southerly conveyor determined the location of the effective Rossby wave source and that the extratropical response is relatively insensitive to the location of the tropical forcing, provided that the tropical response can reach the southerly conveyor. A stronger southerly flow favors a stronger extratropical response, and the spatial structure of the extratropical response is determined by the extratropical westerly basic flows. This result agrees well with Sato and Takahashi (2006), that the appearance of the Rossby wave on the westerly jet is clearly phase-dependent, and may be dominated by the internal

dynamics of interaction between the anomaly pattern and the basic flows. This implies that the anomalous convectivity over the Indian Ocean, or diabatic heating from the ISM, excites a Rossby wave response in the extratropical westerly by triggering the anomalous southerly in the tropics, thus affecting the wavelike pattern on the jet. However, these results were achieved based on a simple barotropic model or statistical analysis, and the real atmosphere is much more complicated. The impact of tropical activity on the wavelike pattern on the jet is still affirmative.

## 6. Conclusions

Using the latest daily observation rainfall data sets for the period 1961–2008, the trend and interannual variations of JJAS mean rainfall in northern China have been studied. Atmospheric circulation anomalies associated with the interannual variation of summer rainfall have also been explored. The major findings are summarized as follows.

Firstly, the RVR of the JJAS rainfall in northern China over the period 1961–2008 shows a “west–increase–east–decrease” pattern, with considerable anomalies over Xinjiang Province and North China. Secondly, the spatial and temporal structures of the interannual variation of JJAS mean rainfall in northern China were revealed by REOF analysis. The first two dominant modes showed a quasi-zonal tripole-like pattern, with the centers over the transition areas of ASAR in northern China. Three regional divisions were identified by the REOF analysis: NC, NEC, and TDNWC. Results indicated that the variation frequency of the summer rainfall anomaly varies between regions. Summer rainfall over NC revealed two dominant variation frequencies and a remarkable dry period from the late 1990s. Over NEC, decadal-scale variation and a decreasing trend in the last two decades was found, but with no significant frequency variation. TDNWC exhibited large interannual variability.

This study has also demonstrated that interannual variations of JJAS mean rainfall in northern China are well related to the upper-level CGT in boreal summer, especially in NC and NEC. The significant summer rainfall anomalies related to the CGT were found to be closely connected with the locations of the action centers of the CGT. There are three center cells of the CGT primarily over East Asia, mainly in northern China, which affect moisture transportation and ascending motion over these regions. Results showed that a positive CGTI will excite a southerly anomaly, bringing more moisture to northern China; meanwhile, upper-level divergence favors low-level convergence and ascending motion over

NC/NEC. As such, positive rainfall anomalies tend to be found in NC/NEC. The correlation coefficients of the regional averaged JJAS mean rainfall over NC and NEC with the CGTI were up to 0.50 and 0.53, respectively, both beyond the 99% confidence level.

The CGT pattern reveals a geographically phase-locked structure during boreal summer from July to September (Ding and Wang, 2005) and is accompanied by significant climate anomalies along its path. This is confirmed by the present study. The closely in-phase relationship between the rainfall anomalies in NC/NEC and the teleconnection patterns provides us with a new way to understand the persistent drought in NC and the decreasing rainfall in NEC. Finally, what contributes to the long-term negative phase of CGTI, and whether the wavelike pattern is the dominant factor contributing to the long-term decrease in northern China, which remain unclear and require further investigation.

**Acknowledgements.** The authors are grateful to Dr. Shang-Ping XIE, Dr. WU Renguang, and the two anonymous reviewers for their insightful comments that led to a significant improvement of the manuscript. This work was supported by the CAS Innovation Key Program (Grant No. KZCX2-YW-BR-14), National Basic Research Program of China (2011CB309704), Special Scientific Research Project for Public Interest (Grant No. GYHY201006021), and the National Natural Science Foundation of China (Grant Nos. 40890155, 40775051, U0733002).

## REFERENCES

- Ambrizzi, T., B. Hoskins, and H. Hsu, 1995: Rossby wave propagation and teleconnection patterns in the austral winter. *J. Atmos. Sci.*, **52**, 3661–3672.
- Chen, L., M. Dong, and Y. Shao, 1992: The characteristics of interannual variations on the East Asian monsoon. *J. Meteor. Soc. Japan*, **70**, 397–421.
- Chen, W., D. Zhu, H. Liu, and S. Sun, 2009: Land-air interaction over arid/semi-arid areas in China and its impact on the east Asian summer monsoon. Part I: Calibration of the land surface model (BATS) using multicriteria methods. *Adv. Atmos. Sci.*, **26**, 1088–1098, doi: 10.1007/s00376-009-8187-3.
- Ding, Q., and B. Wang, 2005: Circumglobal teleconnection in the Northern Hemisphere summer. *J. Climate*, **18**, 3483–3505.
- Ding, Y., Z. Wang, and Y. Sun, 2008: Inter-decadal variation of the summer precipitation in East China and its association with decreasing Asian summer monsoon. Part I: Observed evidences. *Int. J. Climatol.*, **28**, 1139–1161.
- Endo, N., B. Ailikun, and T. Yasunari, 2005: Trends in precipitation amounts and the number of rainy days and heavy rainfall events during summer in China from 1961 to 2000. *J. Meteor. Soc. Japan*, **83**, 621–631.
- Enomoto, T., 2004: Interannual variability of the Bonin high associated with the propagation of rossby waves along the Asian jet. *J. Meteor. Soc. Japan*, **82**, 1019–1034.
- Enomoto, T., B. Hoskins, and Y. Matsuda, 2003: The formation mechanism of the Bonin high in August. *Quart. J. Roy. Meteor. Soc.*, **129**, 157–178.
- Gong, D., P. Shi, and J. Wang, 2004: Daily precipitation changes in the semi-arid region over northern China. *Journal of Arid Environments*, **59**, 771–784.
- Huang, G., 2006: Global climate change phenomenon associated with the droughts in North China. *Climatic and Environmental Research*, **11**, 270–279. (in Chinese)
- Huang, R. H., Y. H. Xu, and L. T. Zhou, 1999: The inter-decadal variation of summer precipitations in China and the drought trend in North China. *Plateau Meteorology*, **18**, 465–476. (in Chinese)
- Huang, R. H., L. Gu, J. L. Chen, and G. Huang, 2008: Recent progresses in studies of the temporal-spatial variations of the east asian monsoon system and their impacts on climate anomalies in China. *Chinese J. Atmos. Sci.*, **32**, 691–719. (in Chinese)
- Kalnay, E., and Coauthors, 1996: The NCEP/NCAR 40-year reanalysis project. *Bull. Amer. Meteor. Soc.*, **77**, 437–471.
- Krishnan, R., and M. Sugi, 2001: Baiu rainfall variability and associated monsoon teleconnections. *J. Meteor. Soc. Japan*, **79**, 851–860.
- Li, X., Y. Zhu, and W. Qian, 2002: Spatiotemporal variations of summer rainfall over eastern China during 1880–1999. *Adv. Atmos. Sci.*, **19**, 1055–1068.
- Liu, Z., and S. Yu, 1993: The upper tropospheric low-frequency waveguides in summer. *Journal of Tropical Meteorology*, **9**, 142–149. (in Chinese)
- Lu, R., J. Oh, and B. Kim, 2002: A teleconnection pattern in upper-level meridional wind over the North African and Eurasian continent in summer. *Tellus A*, **54**, 44–55.
- Ma, Z., and C. Fu, 2006: Some evidences of drying trend over North China from 1951 to 2004. *Chinese Science Bulletin*, **51**, 2913–2925.
- Murata, A., 1990: Regionality and periodicity observed in rainfall variations of the Baiu season over Japan. *Int. J. Climatol.*, **10**, 627–646.
- Nitta, T., and Z. Hu, 1996: Summer climate variability in China and its association with 500 hPa height and tropical convection. *J. Meteor. Soc. Japan*, **74**, 425–445.
- Richman, M., 1986: Rotation of principal components. *Int. J. Climatol.*, **6**, 293–335.
- Rodwell, M., and B. Hoskins, 1996: Monsoons and the dynamics of deserts. *Quart. J. Roy. Meteor. Soc.*, **122**, 1385–1404.
- Sato, N., and M. Takahashi, 2006: Dynamical processes related to the appearance of quasi-stationary waves

- on the subtropical jet in the midsummer northern hemisphere. *J. Climate*, **19**, 1531–1544.
- Shi, S. F., and R. Y. Lu, 2010: Teleconnection patterns along the Asian jet associated with different combinations of convection oscillation over the Indian continent and western North Pacific during summer. *Atmos. Oceanic Sci. Lett.*, **3**, 14–18.
- Shi, Y., Y. Shen, E. Kang, D. Li, Y. Ding, G. Zhang, and R. Hu, 2007: Recent and future climate change in northwest China. *Climatic Change*, **80**, 379–393.
- Wang, B., R. Wu, and K. Lau, 2001: Interannual variability of the Asian summer monsoon: Contrasts between the Indian and the western North Pacific-East Asian monsoons. *J. Climate*, **14**, 4073–4090.
- Wang, W., and K. Li, 1990: Precipitation fluctuation over semiarid region in northern China and the relationship with El Niño/Southern Oscillation. *J. Climate*, **3**, 769–783.
- Wang, Z., C. Chang, B. Wang, and F. Jin, 2005: Teleconnections from Tropics to northern extratropics through a southerly conveyor. *J. Atmos. Sci.*, **62**, 4057–4070.
- Wu, R., and B. Wang, 2002: A contrast of the east Asian summer monsoon-ENSO relationship between 1962–77 and 1978–93. *J. Climate*, **15**, 3266–3279.
- Xu, G., X. Yang, and X. Sun, 2005: Interdecadal and interannual variation characteristics of rainfall in North China and its relation with the northern hemisphere atmospheric circulations. *Chinese Journal Geophysics*, **48**, 511–518. (in Chinese)
- Xue, Y., 1996: The impact of desertification in the Mongolian and the inner Mongolian grassland on the regional climate. *J. Climate*, **9**, 2173–2189.
- Yang, L., and Q. Zhang, 2008: Interannual variation of summer precipitation in Xinjiang and Asian subtropical westerly jet stream. *Journal of Applied Meteorological Science*, **19**, 171–179. (in Chinese)
- Yatagai, A., and T. Yasunari, 1994: Trends and decadal-scale fluctuations of surface air temperature and precipitation over China and Mongolia during the recent 40 year period(1951–1990). *J. Meteor. Soc. Japan*, **72**, 937–957.
- Yatagai, A., and T. Yasunari, 1995: Interrannual variations of summer precipitation in the arid/semi-arid regions in China and Mongolia: Their regionality and relation to the Asian summer monsoon: Special edition on HEIFE. I. *J. Meteor. Soc. Japan*, **73**, 909–923.
- Zhang, J., W. Dong, and C. Fu, 2005: Impact of land surface degradation in northern China and southern Mongolia on regional climate. *Chinese Science Bulletin*, **50**, 75–81.
- Zhou, L., and R. Huang, 2009: Interdecadal variability of summer rainfall in Northwest China and its possible causes. *Int. J. Climatol.*, **30**, 549–557.
- Zhou, L. T., and R. H. Huang, 2006: Characteristics of interdecadal variability of the difference between surface temperature and surface air temperature in spring in arid and semi-arid region of Northwest China and its impact on summer precipitation in North China. *Climatic and Environmental Research*, **11**, 1–13. (in Chinese)